overall body coloration ($t_{26} = 0.48$, $P = 0.63$; all individual components not significant). The analysis of body coloration was done blind of paternity assignment (see below).

Artificial insemination

Male guppies produce sperm packaged in bundles (spermatozeugmata). In preliminary trials, 23 males were repeatedly stripped to obtain three independent measures for the number of sperm per bundle for each male (for two males only two counts were obtained). Analysis of variance (with males as random factors) revealed that between-male variation in the number of sperm per bundle did not exceed that observed within individuals (analysis of variance (ANOVA): $F_{22,44} = 0.76$, $P = 0.76$). The number of sperm per bundle was not significantly correlated with any of the morphological traits measured in this study (orange: $r = 0.20$, $P = 0.35$; blue: $r = 0.14$, $P = 0.52$; black: $r = 0.03$, $P = 0.91$; body size: $r = 0.03$, $P = 0.88$, $n = 23$). In each trial, equal numbers of bundles were obtained from each of the two males[27], gently mixed and inseminated simultaneously into an anaesthetized female using a machine-pulled micropipette (penetration depth approximately 2 mm). The number of sperm inseminated was based on the size of natural ejaculates in the study population ($\sim 0.5 \times 10^6$ spermatozoa) (see also ref. 20). After artificial insemination, females were revived and isolated until they produced their first brood. Tissue samples were obtained from all fish (mother, two putative sires and offspring) for the subsequent paternity analysis.

Paternity analysis

We observed no offspring mortality before paternity assignment. Two microsatellite markers (accession numbers: AF164205 and AF026459) were used to estimate each male's relative share of paternity (P_B). The polymerase chain reaction (PCR) protocol followed previous work[8] with the exception that one primer from each pair was end-labelled with a fluorescent phosphoramidite dye. Amplified fragments were separated by electrophoresis on an ABI 3100 sequencer (ABI PRISM), using 400 HD ROX (Perkin-Elmer) as a size standard. PCR products were visualized using Genographer software (v. 1.6.0) and paternity was assigned to offspring according to allele sharing between putative sires, mother and offspring. Both loci were highly variable (18 and 33 alleles, with expected heterozygosities of 0.901 and 0.941 respectively) and exhibited a global exclusion probability of 0.92. Where one parent (the mother) is known, paternity assignment with two putative sires (as in our study) is calculated to be 100% (Cervus v. 2.0)[28]. In practice, paternity was unambiguously assigned to all offspring ($n = 300$ from 27 broods).

Data analysis

The James method[16] was used to test whether the proportion of offspring sired by the male labelled B fluctuates randomly between families (with different brood sizes)[29], and thus whether the observed P_B variance deviates from binomial expectation. A generalized linear model with binomial errors and logit link function was then used to determine whether male phenotype accounted for deviance in P_B. For each family, male B success (the number of offspring sired by male B) and the total number of offspring were entered as the binomial response variables. Predictor variables, representing differences in the phenotypic trait measurements taken from the two males per family (male B trait minus male A trait), were fitted into the model. Initially, the full model included all possible explanatory variables; the term with the least significant probability was then excluded in a stepwise procedure. The change in deviance in the generalized linear model resulting from the removal of each term was tested against an F-distribution. We removed all terms whose exclusion did not cause a significant change in the deviation of the model (Table 1).

Received 18 October; accepted 10 December 2002; doi:10.1038/nature01367.

1. Parker, G. A. in *Sperm Competition and Sexual Selection* (eds Birkhead, T. R. & Møller, A. P.) 3–54 (Academic, San Diego, 1998).
2. Eberhard, W. G. *Female Control: Sexual Selection by Cryptic Female Choice* (Princeton Univ. Press, Princeton, 1996).
3. Birkhead, T. R. & Pizzari, T. Postcopulatory sexual selection. *Nature Rev. Genet.* **3,** 262–273 (2002).
4. Birkhead, T. R. & Møller, A. P. (eds) *Sperm Competition and Sexual Selection* (Academic, San Diego, 1998).
5. Birkhead, T. R. Defining and demonstrating postcopulatory female choice—again. *Evolution* **54,** 1057–1060 (2000).
6. Simmons, L. W. *Sperm Competition and its Evolutionary Consequences in the Insects* (Princeton Univ. Press, Princeton, New Jersey, 2001).
7. Dziuk, P. J. Factors that influence the proportion of offspring sired by a male following heterospermic insemination. *Anim. Reprod. Sci.* **43,** 65–68 (1996).
8. Evans, J. P. & Magurran, A. E. Patterns of sperm precedence and predictors of paternity in the Trinidadian guppy. *Proc. R. Soc. Lond. B* **268,** 719–724 (2001).
9. Sheldon, B. C. Male phenotype, fertility, and the persuit of extra-pair copulations by female birds. *Proc. R. Soc. Lond. B* **257,** 25–30 (1994).
10. Blount, J. D., Møller, A. P. & Houston, D. C. Antioxidants, showy males and sperm quality. *Ecol. Lett.* **4,** 393–396 (2001).
11. Jennions, M. D. & Petrie, M. Why do females mate multiply? A review of the genetic benefits. *Biol. Rev.* **75,** 21–64 (2000).
12. Evans, J. P. & Magurran, A. E. Multiple benefits of multiple mating in guppies. *Proc. Natl Acad. Sci. USA* **97,** 10074–10076 (2000).
13. Houde, A. E. *Sex, Color, and Male Choice in Guppies* (Princeton Univ. Press, Princeton, New Jersey, 1997).
14. Endler, J. A. & Houde, A. E. Geographical variation in female preferences for male traits in *Poecilia reticulata*. *Evolution* **49,** 456–468 (1995).
15. Reynolds, J. D. & Gross, M. R. Female mate preference enhances offspring growth and reproduction in a fish. *Poecilia reticulata*. *Proc. R. Soc. Lond. B* **264,** 57–62 (1992).
16. James, W. H. The distribution of the combinations of the sexes in mammalian litters. *Genet. Res.* **26,** 45–53 (1975).
17. Constantz, G. D. in *Ecology and Evolution of Livebearing Fishes* (eds Meffe, G. K. & Snelson, Jr F. F.) 33–50 (Prentice-Hall, New Jersey, 1989).
18. Endler, J. A. Natural and sexual selection on colour patterns in poeciliid fishes. *Environ. Biol. Fishes* **9,** 173–190 (1983).
19. Houde, A. E. Mate choice based on naturally occurring colour-pattern variation in a guppy population. *Evolution* **41,** 1–10 (1987).
20. Pilastro, A., Evans, J. P., Sartorelli, S. & Bisazza, A. Male phenotype predicts insemination success in guppies. *Proc. R. Soc. Lond. B* **269,** 1325–1330 (2002).
21. Pizzari, T. & Birkhead, T. R. Female feral fowl eject sperm of subdominant males. *Nature* **405,** 787–789 (2000).
22. Lewis, S. M. & Austad, S. N. Sexual selection in four beetles: the relationship between sperm precedence and male olfactory attractiveness. *Behav. Ecol.* **5,** 219–224 (1994).
23. Edvardsson, M. & Arnqvist, G. Copulatory courtship and cryptic female choice in red flour beetles *Tribolium castaneum*. *Proc. R. Soc. Lond. B* **267,** 559–563 (2000).
24. Zeh, J. A. & Zeh, D. W. The evolution of polyandry II: post-copulatory defences against genetic incompatibility. *Proc. R. Soc. Lond. B* **264,** 69–75 (1997).
25. Harvey, I. F. & Parker, G. A. 'Sloppy' sperm mixing and intraspecific variation in sperm precedence (P_2) patterns. *Proc. R. Soc. Lond. B* **267,** 2537–2542 (2000).
26. Neems, R. M., Lazarus, J. & McLachlan, A. J. Lifetime reproductive success in a swarming midge: trade-offs and stabilizing selection for male body size. *Behav. Ecol.* **9,** 279–286 (1998).
27. Matthews, I. M., Evans, J. P. & Magurran, A. E. Male display rate reveals ejaculate characteristics in the Trinidadian guppy *Poecilia reticulata*. *Proc. R. Soc. Lond. B* **264,** 695–700 (1997).
28. Marshall, T. C., Slate, J., Kruuk, L. E. B. & Pemberton, J. M. Statistical confidence for likelihood-based paternity inference in natural populations. *Mol. Ecol.* **7,** 639–655 (1998).
29. Krackow, S., Meelis, F. & Hardy, I. C. W. in *Sex Ratios: Concepts and Research Methods* (ed. Hardy, I. C. W.) 112–131 (Cambridge Univ. Press, Cambridge, UK, 2002).
30. Williams, D. A. Extra-binomial variation in logistic linear models. *Appl. Stat.* **31,** 144–148 (1982).

Acknowledgements We thank T. Birkhead, J. Kelley, B. Kempenaers, F. Neat, T. Pizzari, L. Simmons and A. Skinner for comments on an earlier draft of the manuscript, C. Romualdi for statistical advice and A. Ludlow for assistance with the preliminary artificial insemination trials. This research was supported by a Marie Curie Independent Research Fellowship from the EU and was carried out in conformity with the relevant Italian laws governing the care of animals in research.

Competing interests statement The authors declare that they have no competing financial interests.

Correspondence and requests for materials should be addressed to J.P.E. (e-mail: jonathan.evans@unipd.it).

Comparative power curves in bird flight

B. W. Tobalske*, T. L. Hedrick†, K. P. Dial‡ & A. A. Biewener†

* *Department of Biology, University of Portland, 5000 North Willamette Boulevard, Portland, Oregon 97203, USA*
† *Concord Field Station, Harvard University, Old Causeway Road, Bedford, Massachusetts 01738, USA*
‡ *Division of Biological Sciences, University of Montana, Missoula, Montana 59812, USA*

The relationship between mechanical power output and forward velocity in bird flight is controversial, bearing on the comparative physiology and ecology of locomotion[1,2]. Applied to flying birds, aerodynamic theory predicts that mechanical power should vary as a function of forward velocity in a U-shaped curve. The only empirical test of this theory, using the black-billed magpie (*Pica pica*), suggests that the mechanical power curve is relatively flat over intermediate velocities[3]. Here, by integrating *in vivo* measurements of pectoralis force and length change with quasi-steady aerodynamic models developed using data on wing and body movement, we present mechanical power curves for cockatiels (*Nymphicus hollandicus*) and ringed turtle-doves (*Streptopelia risoria*). In contrast to the curve reported for magpies[3], the power curve for cockatiels is acutely concave, whereas that for doves is intermediate in shape and shows higher mass-specific power output at most speeds. We also find that wing-beat frequency and mechanical power output do not

necessarily share minima in flying birds. Thus, aspects of morphology, wing kinematics and overall style of flight can greatly affect the magnitude and shape of a species' power curve.

We integrated several techniques to study *in vivo* mechanical power output from the pectoralis, the primary flight muscle in birds, as a function of forward flight velocity. We flew cockatiels and doves in a variable-speed wind tunnel and measured wing and body movements in three dimensions simultaneously with direct measures of force development and length change of the pectoralis. The three-dimensional (3D) kinematic data were incorporated into a model of quasi-steady aerodynamic power output, which we developed using existing theory[4–6]. Pectoralis tension and length change were measured using bone-strain recordings and sonomicrometry, respectively (ref. 7 and Fig. 1a). Our aerodynamic model, coupled with observed changes in muscle length, was used to calibrate measurements of bone strain into units of muscle force at intermediate speeds (7 and 9 m s^{-1}). These force calibrations were then applied to bone-strain data at all flight speeds.

To estimate work output per wing beat, we integrated tension-length curves, or work loops, for each wing beat (Fig. 1b). Average power output from the pectoralis muscles was then calculated as total work during an interval of flight divided by flight duration. Pectoralis power output varied significantly with flight speed in both species (repeated-measures analysis of variance, $P \leq 0.002$; Fig. 2a, b). In the cockatiels, minimum power output was 1.3 W (73.9 W kg^{-1} muscle mass) at 5 m s^{-1}, and maximum power output was 3.7 W (231.2 W kg^{-1}) at 14 m s^{-1}, the fastest speed at which the cockatiels would fly. In the doves, minimum power (4.3 W; 123.4 W kg^{-1}) was observed at 7 m s^{-1}, and maximum power output (7.5 W; 234.5 W kg^{-1}) was observed at this species' maximum flight speed of 17 m s^{-1}. Mass-specific power output in the dove was higher than that for the cockatiel at all speeds except 14 m s^{-1}. This is probably due to the higher weight per area swept by the wings (disc loading) of the dove (8.1 N m^{-2}) as compared with the cockatiel (4.2 N m^{-2}) and therefore to the proportionally greater induced power requirements of the dove.

Our results do not support a current hypothesis that minimum wing-beat frequency must coincide with a bird's minimum power speed[8]. For cockatiels and doves, relative work varied closely with relative power, and both variables showed shared minima (Fig. 3b, c). By contrast, wing-beat frequency in cockatiels reached a well-defined minimum at 9 m s^{-1}, a speed 80% higher than their minimum power speed, whereas wing-beat frequency in doves showed a broad minimum from 7 to 13 m s^{-1}.

Power curves in doves and cockatiels differed substantially from the curve measured in magpies, the only other species for which similar muscle measurements have been made over a range of flight

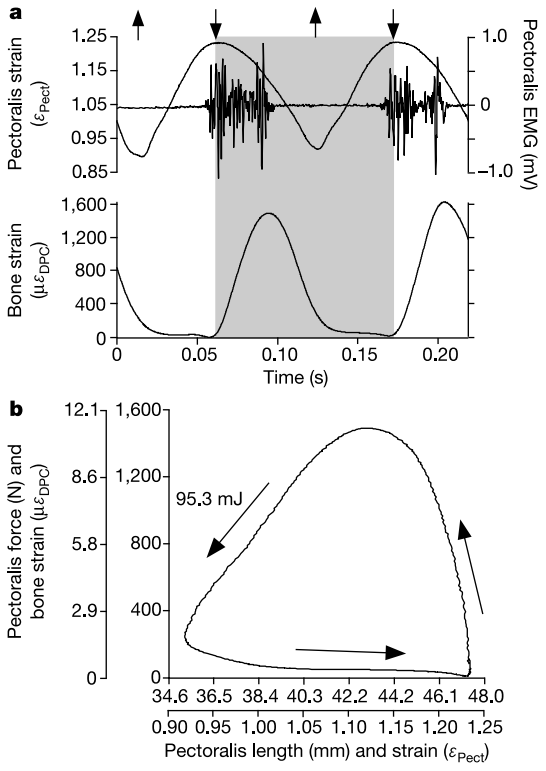

Figure 1 *In vivo* recordings of pectoralis strain, force and work per wing-beat cycle. **a**, Changes in muscle length, electromyographic (EMG) activity and bone strain recorded from a cockatiel flying at 7 m s^{-1}. Shaded region indicates a single wing-beat cycle selected for plotting as a tension-length curve (work loop in **b**). Arrows indicate upstroke and downstroke. **b**, Work loop plotted from a single wing beat (shaded region in **a**). We calibrated bone and pectoralis strain into pectoralis force and length using our aerodynamic model and the bird's morphology. The integral of the work loop (95.3 mJ) was divided by time (112.2 ms) to yield power for a single pectoralis (0.85 W), and this value was doubled to yield total pectoralis power (1.7 W or 106 W kg^{-1} pectoralis mass) for the wing beat.

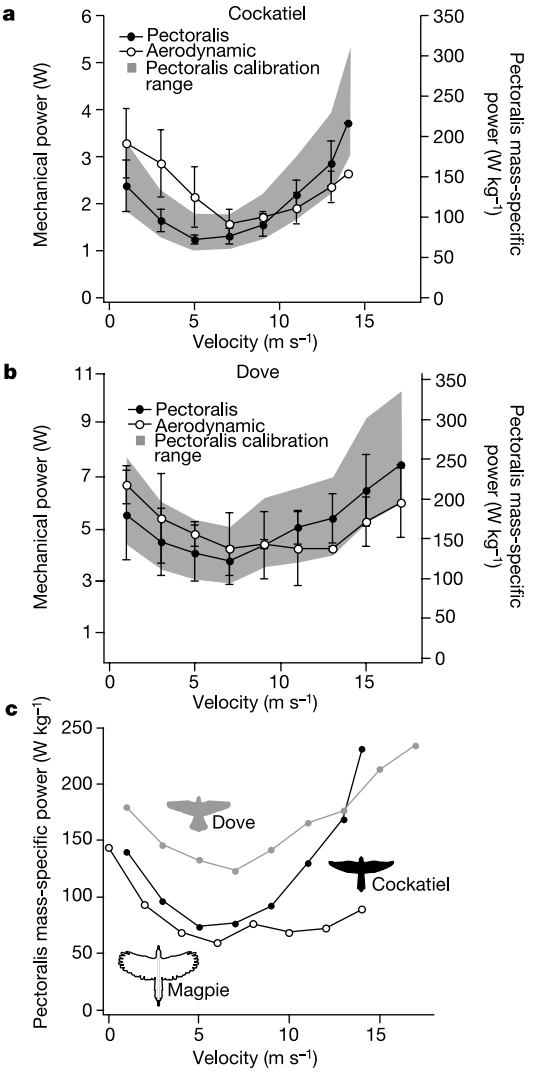

Figure 2 Pectoralis power as a function of flight velocity. **a**, **b**, Mean ± s.d. pectoralis and aerodynamic power as a function of flight velocity in five cockatiels (**a**) and three doves (**b**). In both cases, the shaded region indicates the range of pectoralis power obtained when 'low-power' versus 'high-power' aerodynamic coefficients are input to the aerodynamic model (Methods). **c**, Comparative mass-specific pectoralis power as a function of flight velocity in cockatiels, doves and magpies[3]. Bird silhouettes are shown to scale, digitized from video.

speeds[3]. Differences in calibration method for strain-gauge measurements cannot account for all of the interspecific differences because relative power curves varied between the species (Fig. 3a), and relative power and work (Fig. 3b, c) were independent of force calibration.

As compared with the mechanical power curve for the magpie, which has a broadly flat shape between 4 and 12 m s^{-1}, progressively greater upward concavity was apparent for the curves shown by doves and cockatiels, respectively (Figs 2c and 3a). Maximum mass-specific pectoralis power output in cockatiels and doves was 63% higher than the maximum of 143 W kg^{-1} previously reported for magpies[3]. Unlike the cockatiels and doves, magpies are reported to generate maximal pectoralis power during hovering[3]. We attribute these differences in the shape and magnitude of the power curves to differences in wing and tail morphology.

Magpies have broad, rounded wings (aspect ratio 5) and a long tail. This probably increases profile drag, diminishes thrust/drag ratio[2] and prevents them from flying faster than 14 m s^{-1}, even though they seem to have sufficient pectoralis power to fly at faster speeds. By contrast, cockatiels and doves have relatively pointed wings of higher aspect ratio (7.0 and 5.7) and proportionally smaller tails. These characteristics offer proportionally lower induced velocities and profile drag and, thus, more favourable thrust/drag ratios, permitting them to fly at speeds that require pectoralis power output in excess of that required for hovering. Unlike in magpies, maximum speed in cockatiels and doves is probably constrained by sustainable power available from the pectoralis muscle.

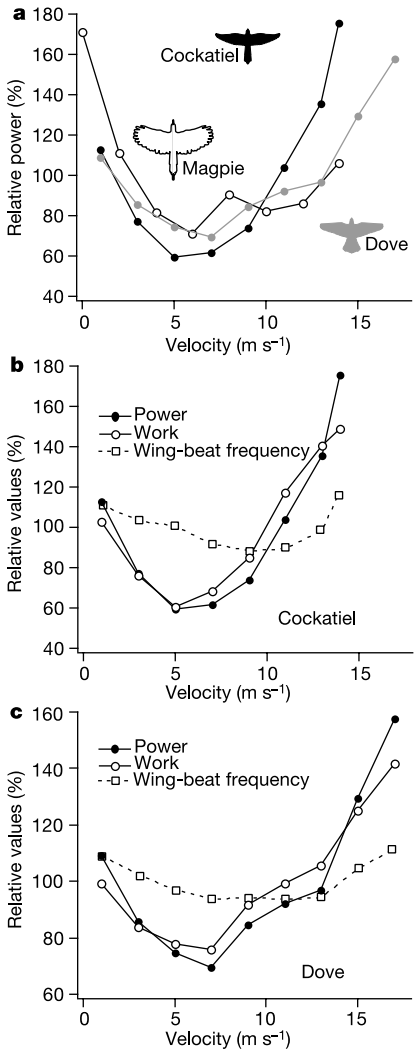

Figure 3 Pectoralis power, work and wing-beat frequency as a function of flight velocity, with values expressed as a percentage of the observed within-species mean for each variable. **a**, Mean relative pectoralis power in cockatiels, doves and magpies[7]. **b**, **c**, Mean relative pectoralis power, work and wing-beat frequency in cockatiels (**b**) and doves (**c**).

Differences in power curves between magpies and the species in the present study may also be explained by flight style. Magpies use a unique intermittent flight style in which they regularly fluctuate their wing-beat gait, flight velocity and altitude[9]. This variation in wing motion may alter power requirements at intermediate and fast speeds so that the right side of the power curve remains relatively flat for this species.

Maximum mass-specific pectoralis power output in the cockatiel and dove was 60% or less than values (360–460 W kg^{-1}) that have been estimated for galliform species (pheasant-like birds) engaged in short-duration take-off and climbing flight[6]. In those studies, flight style and speed range differed, but similar aerodynamic modelling and sonomicrometry methods were used. Thus, we attribute most of the interspecific variation between these studies to differences in non-sustainable versus sustainable flight performance and flight morphology. Among all species of birds, galliforms seem to be designed for maximum burst-flight performance: they have short, broad wings, high wing-beat frequency and pectoralis muscles with fast myosin ATPase and high glycolytic capacity[10–12]. They use flight almost only as an escape mechanism, rapidly fatiguing after take-off and returning to the ground to run or hide, whereas cockatiels and doves may sustain flight for hours before fatigue.

Data from the cockatiels and doves provide insight into the validity of certain assumptions in quasi-steady aerodynamics as applied to bird flight. Because we used aerodynamic estimates of power output at intermediate flight speeds to calibrate bone strain into muscle force, by necessity the curves for aerodynamic power and pectoralis power intersect in the vicinity of 7–9 m s^{-1} for both species (Fig. 2a, b). But pectoralis power was not constrained to match aerodynamic power at slower or faster speeds. It is therefore significant that our measurements of aerodynamic power overestimate pectoralis power at slow speeds and underestimate pectoralis power at fast speeds in both species. Several explanations could account for these discrepancies. Wing muscles other than the pectoralis may contribute significantly to work and power during slow flight[13], and we did not measure power output in these muscles. In addition, our model accounts only for the wings; other lift surfaces, especially the tail, may be particularly important for reducing power requirements at slow speeds[14,15]. By contrast, at faster speeds our model seems to underestimate drag. Drag coefficients on bird wings and bodies are subject to much uncertainty[8]. Without more definitive estimates for these parameters and induced velocity, we are unable to determine which components of total drag were underestimated.

In summary, our data show that differences in morphology, wing kinematics and overall style of flight have large effects on the magnitude and shape of a species' power curve. □

Methods

Birds, kinematic analysis and aerodynamic modelling

Five cockatiels (body mass 78.5 g, wing span 48.3 cm) and three doves (139.8 g, 46.8 cm) were trained to fly individually in a variable-speed wind tunnel at the Concord Field Station, Harvard University (41-m altitude, average air density (ρ) 1.22 kg m^{-3}). We followed Institutional Animal Care and Use guidelines in all housing and experiment protocols. The working-section diameter of the tunnel was 1.2 × 1.2 m (ref. 15). We report equivalent air speed V_e rather than true air speed[16]:

$$V_e = \sqrt{2q/\rho_o} \quad (1)$$

where q is dynamic pressure and ρ_o is the air density at sea level (1.225 kg m^{-3}). The birds were trained to sustain flight indefinitely at intermediate speeds (5–11 m s^{-1}) and for at least 20 s at other speeds. Kinematic data were obtained using 2–4 synchronized, 250-Hz digital video cameras (n = 214 wing beats for cockatiels, n = 98 for doves). We merged two-dimensional coordinates from each camera plane into a single 3D coordinate space using the direct linear transformation (DLT) coefficients derived from a 40-point calibration frame[15]. Variables obtained from the kinematic analyses were used in constructing quasi-steady aerodynamic models incorporating actuator-disc theory and

strip analysis[4–6]. Relative to free-stream velocity, we measured body angle, wing span, wing elevation, stroke-plane angle of the wing and angular velocity of the wing. Total aerodynamic power (P_{aero}) was calculated as the sum of induced P_{ind}, profile P_{pro} and parasite P_{par} power, and rate change in potential energy. Inertial power, added mass and rate change in kinetic energy were ignored. For the aerodynamic variables contributing to P_{aero}:

$$P_{ind} = M_b k w (g + A_v) \quad (2)$$

where M_b is body mass, k is the induced velocity correction factor (assumed to be 1.2), w is induced velocity, g is gravitational acceleration, and A_v is vertical acceleration. In our calculation of w, we defined disc area as the area swept by the wings, not a circle[6].

$$P_{pro} = 2\sum_{i=1}^{25}\left(\frac{1}{2}\rho V_{R,i} S_i C_{D,pro}\right) \quad (3)$$

where V_R is the resultant velocity of a given wing strip, S is the surface area of a wing strip, and $C_{D,pro}$ is the profile drag coefficient (assumed to be 0.02)[4,5]. We assumed no change in average wing chord throughout the wing-beat cycle.

$$P_{par} = \frac{1}{2}\rho S_b C_{D,par} V_e^3 \quad (4)$$

where S_b is the projected equivalent flat-plate area of body, calculated incorporating body angle relative to free-stream flow[4], and $C_{D,par}$ is the parasite drag coefficient (assumed to be 0.13)[2,6].

Bone strain and muscle length

Using surgically implanted strain gauges and sonomicrometry crystals, we obtained *in vivo* measurements of bone strain (ε_{DPC}) and pectoralis strain (ε_{Pect}; Fig. 1a). Strains were defined with resting (initial) length as that during perching with the bird motionless. A single-element, 1-mm metal-foil strain gauge was placed perpendicular to the long axis of the humerus on the dorsal surface of the delto-pectoral crest (DPC), the insertion for the pectoralis. We assumed that ε_{DPC} is proportional to muscle tension. Two 1-mm sonomicrometry crystals (resolution $\pm$ 15 μm) were placed 2.5-mm deep, 15-mm apart into the longest fascicles of the mid-belly, the pars sternobrachialis of the pectoralis. We used indwelling electromyography electrodes to measure the timing of pectoralis activity (Fig. 1a).

Calculating pectoralis work and power

Within each wing beat sampled (n = 979 wing beats for cockatiels, n = 1,067 for doves), we integrated the curve of ε_{DPC} plotted as a function of ε_{Pect}. The area of these dimensionless loops was converted into work (J) per wing beat by multiplyng ε_{Pect} by L_{rest}, the resting fascicle length (m) of the pectoralis in the region implanted with sonomicrometry crystals, and by multiplying ε_{DPC} by F, a force calibration factor (Fig. 1b). We avoided exclusive reliance on our earlier "pull-calibration" technique[3,7] because we were unable to obtain consistent calibrations in individuals of both species: pull calibrations yielded an average coefficient of variance for F of 29.0 $\pm$ 14.7% in individual birds. Owing to the superficial application of tensile force, this approach also probably engenders larger bending moments than *in vivo* forces transmitted by the muscle at its attachment site, leading to an underestimate of F. Because of these concerns, F was calculated so that mechanical power in the paired pectoralis was set to equal P_{tot} for the subset of wing beats for which kinematics were analysed at 7 and 9 m s^{-1} (n = 63 for cockatiels, n = 29 for doves). These speeds were chosen because flight at slower speeds is more likely to violate our assumption of quasi-steady flow[13], and P_{aero} at faster speeds is more sensitive to assumed values of $C_{D,pro}$ and $C_{D,par}$. For each bird, pectoralis power, P_{pect}, was calculated as total work output at a given speed divided by total time in flight at that speed. This approach yielded more consistent calibrations (cv = 10.2 $\pm$ 4.2%) for F in individual birds.

To evaluate the sensitivity of our aerodynamic-calibration approach, we varied the values of k, $C_{D,pro}$ and $C_{D,par}$ for a low- versus a high-power case. In the low-power case, k was decreased from 1.2 to 1.0, and $C_{D,par}$ and $C_{D,pro}$ were decreased by 50% to 0.065 and 0.01, respectively; for the high-power case, k was assumed to be 1.4, and $C_{D,par}$ and $C_{D,pro}$ were increased by 50% to 0.195 and 0.03. This allowed us to bracket the likely range of pectoralis power that might be observed at any particular flight speed (Fig. 2a, b). We also computed relative power, work and wing-beat frequency, all independent of F, by dividing the observed values in physical units by their respective within-species means and multiplying the dimensionless results by 100 to obtain percentages (Fig. 3).

Received 29 July; accepted 29 October 2002; doi:10.1038/nature01284.

1. Ellington, C. P. Limitations on animal flight performance. *J. Exp. Biol.* **160,** 71–91 (1990).
2. Rayner, J. M. V. Estimating power curves of flying vertebrates. *J. Exp. Biol.* **202,** 3449–3461 (1999).
3. Dial, K. P., Biewener, A. A., Tobalske, B. W. & Warrick, D. R. Mechanical power output of bird flight. *Nature* **390,** 67–70 (1997).
4. Rayner, J. M. V. A vortex theory of animal flight. Part 2. The forward flight of birds. *J. Fluid Mech.* **91,** 731–763 (1979).
5. Norberg, U. M. *Vertebrate Flight: Mechanics, Physiology, Morphology, Ecology and Evolution* (Springer, Berlin, 1990).
6. Askew, G. N., Marsh, R. L. & Ellington, C. P. The mechanical power output of the flight muscles of blue-breasted quail (*Coturnix coturnix*) during take-off. *J. Exp. Biol.* **204,** 3601–3619 (2001).
7. Biewener, A. A., Corning, W. R. & Tobalske, B. W. *In vivo* muscle force-length behavior during level flight in pigeons (*Columba livia*). *J. Exp. Biol.* **201,** 3293–3307 (1998).
8. Pennycuick, C. J., Klaasen, M., Kvist, A. & Lindström, Å. Wingbeat frequency and the body drag anomaly: wind-tunnel observations on a thrush nightingale (*Luscinia luscinia*) and a teal (*Anas crecca*). *J. Exp. Biol.* **199,** 2757–2765 (1996).
9. Tobalske, B. W. Biomechanics and physiology of gait selection in flying birds. *Physiol. Biochem. Zool.* **73,** 736–750 (2000).
10. Tobalske, B. W. & Dial, K. P. Effects of body size on take-off performance in the Phasianidae (Aves). *J. Exp. Biol.* **203,** 3319–3332 (2000).
11. Rosser, B. W. C. & George, J. C. The avian pectoralis: histochemical characterization and distribution of muscle fiber types. *Can. J. Zool.* **64,** 1174–1185 (1986).
12. Rosser, B. W. C., Wick, M., Waldbillig, D. M. & Bandman, E. Heterogeneity of myosin heavy-chain expression in fast-twitch fiber types of mature avian pectoralis muscle. *Biochem. Cell Biol.* **74,** 715–728 (1996).
13. Dial, K. P. Activity patterns of the wing muscles of the pigeon (*Columba livia*). *J. Exp. Zool.* **262,** 357–373 (1992).
14. Thomas, A. L. R. On the aerodynamics of birds' tails. *Phil. Trans. R. Soc. Lond. B* **340,** 361–380 (1993).
15. Hedrick, T. L., Tobalske, B. W. & Biewener, A. A. Estimates of circulation and gait change based on a three-dimensional kinematic analysis of flight in cockatiels (*Nymphicus hollandicus*) and ringed turtle-doves (*Streptopelia risoria*). *J. Exp. Biol.* **205,** 1389–1409 (2002).
16. Pennycuick, C. J., Alterstam, T. & Hedenström, A. A new low-turbulence wind tunnel for bird flight experiments at Lund University, Sweden. *J. Exp. Biol.* **200,** 1441–1449 (1997).

Acknowledgements We thank G. Lauder and F. Jenkins Jr for comments on this work, and the Concord Field Station staff for animal care and help with experiments. This work was supported by grants from the National Science Foundation to A.A.B. and K.P.D., and from Murdock to B.W.T.

Competing interests statement The authors declare that they have no competing financial interests.

Correspondence and requests for materials should be addressed to B.W.T. (e-mail: tobalske@up.edu).

Neuronal synchrony does not correlate with motion coherence in cortical area MT

Alexander Thiele*† **& Gene Stoner***

* *Salk Institute for Biological Studies, La Jolla, California 92037, USA*

Natural visual scenes are cluttered with multiple objects whose individual features must somehow be selectively linked (or 'bound') if perception is to coincide with reality. Recent neurophysiological evidence[1,2] supports a 'binding-by-synchrony' hypothesis[3]: neurons excited by features of the same object fire synchronously, while neurons excited by features of different objects do not. Moving plaid patterns offer a straightforward means to test this idea. By appropriate manipulations of apparent transparency, the component gratings of a plaid pattern can be seen as parts of a single coherently moving surface or as two non-coherently moving surfaces. We examined directional tuning and synchrony of area-MT neurons in awake, fixating primates in response to perceptually coherent and non-coherent plaid patterns. Here we show that directional tuning correlated highly with perceptual coherence, which is consistent with an earlier study[4]. Although we found stimulus-dependent synchrony, coherent plaids elicited significantly less synchrony than did non-coherent plaids. Our data therefore do not support the binding-by-synchrony hypothesis as applied to this class of motion stimuli in area MT.

To confirm that monkeys' perception is influenced by transparency manipulations[5–8], we trained one monkey to distinguish coherent from non-coherent motion. After training, perceptual reports were obtained for nine probe plaids. For eight of these plaids, we manipulated transparency by holding the intensities of the two gratings (thin bar phase) constant and identical, and varying the intensity of the grating intersections[5–8]. The ninth probe plaid had one bright and one dark grating. We termed this

† Present address: Henry Wellcome Building for Neuroecology, University of Newcastle upon Tyne, NE2 4HH, UK.